

Gluon propagators and quark confinement

K. Langfeld, H. Reinhardt and J. Gattnar

Institut für Theoretische Physik, Universität Tübingen
D-72076 Tübingen, Germany

Abstract

The gluon propagator is investigated in Landau and in maximal center gauge for the gauge group $SU(2)$ by means of lattice gauge simulations. We find that Gribov ambiguities arising from the implementation of Landau gauge have a small influence on the propagator. In agreement with previous findings, we obtain that the small momentum behavior is dominated by a mass, which is of order $(1.48 \pm 0.05) \sqrt{\sigma}$, where σ is the string tension. By removing the confining vortices from the full Yang-Mills ensemble, we convert full YM-theory into a theory which does not confine quarks. We find that in the latter case the strength of the gluon propagator in the intermediate momentum range is strongly reduced. The spectral functions which reproduce the numerical data for the propagators are analyzed using a generalized Maximum Entropy Method.

PACS: 11.15.Ha, 12.38.Aw, 14.70.Dj

keywords: gluon propagator, $SU(2)$ lattice gauge theory, quark confinement, spectral function.

Supported in part by DFG Re856/4-1.

1 Introduction

Nowadays, the general belief that QCD is the correct theory of strong interactions is supported by numerous high energy collisions experiments (see e.g. [1]). At high momentum transfers, at which the effective quark-gluon coupling becomes small, predictions of perturbation theory nicely agree with the experimental data. On the other hand, this coupling becomes large and even diverges at low energies (Landau pole) thus prohibiting a perturbative treatment and pointing towards new phenomena. One might speculate that the strong increase of the effective coupling is the progenitor of quark confinement. Note, however, that a toy quark model which mimics the QCD perturbative behavior of the running coupling strength reveals that the new phenomenon at low energies is quark mass generation (which screens the Landau pole [2]) rather than quark confinement.

One prominent method to treat non-perturbative Yang-Mills theory is the numerical simulation of lattice gauge theory (LGT). LGT covers all non-perturbative effects and, in particular, bears witness of quark confinement (see e.g. [3]). Moreover, the numerical results suggest that, in certain gauges, topological defects act as quark confiners. The presence of these defects is independent of the coupling strength, and their properties are beyond the reach of perturbation theory. In the case of Abelian gauges [4], these defects are chromomagnetic monopoles, which condense and give rise to the dual Meissner effect as confinement scenario [5, 3, 6] (for a caveat see [6]). A generalization of the dual Meissner effect to the non-abelian case was put forward in [7] to resolve the neutral particle problem. In the Center gauges [8], the topological defects are center vortices. The mechanism of quark confinement can be understood as a percolation of center vortices which acquire physical relevance in the continuum limit [9]. Lattice gauge calculations also provide an intuitive picture in terms of vortex physics for the deconfinement phase transition at finite temperatures [10]. Reducing the full Yang-Mills configurations to their vortex content still yields the full string tension [8]. Vice versa, removing these vortices from the Yang-Mills ensemble results in a vanishing string tension [8] and in addition to a restoration of chiral symmetry [11].

Unfortunately, simulations of LGT including dynamical quarks are still cumbersome despite the recent successes by improved algorithms [12] and the increase of computational power. Moreover, at the present stage systems at finite baryon densities are hardly accessible in the realistic case of an SU(3) gauge group [13] (for recent successes see [14]). These deficiencies are over-

come by a second non-perturbative method to treat Yang-Mills theory: the approach by the Dyson-Schwinger equations (DSE). By contrast to the lattice formulation, the DSE approach can easily deal with dynamical quarks and, furthermore, can be easily extended to finite baryon densities [15]. Moreover, it can be used to study hadron phenomenology [16, 17]. The disadvantage of the DSE approach is that it requires a truncation of the infinite tower of equations, and that this approximation is difficult to control and to improve systematically. In addition, the DSE approach needs gauge fixing which is obscured by Gribov copies. Whether the standard Faddeev-Popov method of gauge fixing is appropriate in non-perturbative studies, is still under debate [18].

In view of the importance of the DSE approach for the understanding of hadron physics [16, 17], it is highly interesting to learn more about the impact of truncating the Dyson tower of equations. Since the gluon and ghost propagators are essential ingredients of the quark DSE, these propagators are of particular interest.

In this paper, we will address the gluon propagator in Landau gauge for the simpler case of pure SU(2) lattice gauge theory. The lattice result will be compared with the one provided by the solution of the coupled ghost-gluon Dyson equation [19, 20, 21, 22]. By removing the center vortices from the SU(2) Yang-Mills ensemble, we will focus on the information on quark confinement which might be encoded in the gluon propagator. High accuracy numerical data for the latter are obtained by means of a new numerical method superior to existing techniques.

The organization of the paper is as follows: In section 2, we present the lattice definition of the gluon propagator. For making contact with the ab initio continuum formulation of Yang-Mills theory, we will define the gluon field from the adjoint links. We furthermore outline in this section the gauge fixing procedure. In section 3, we present our numerical results for the gluon propagator in the Landau gauge and the maximal center gauge, respectively. In section 4, we discuss the gluonic spectral function which is extracted from the gluon propagator by using (an extension of) the maximal entropy method. Finally, our conclusions are presented in section 5.

2 The lattice approach to the gluon propagator

In this section, we will extract the gluon propagator of the continuum Yang-Mills theory by considering the continuum limit of the lattice gauge theory. Thereby, we will carefully examine the relation between the lattice link variables and the gauge potential.

2.1 The lattice definition of the gluon field

Before identifying the gluonic degrees of freedom in the lattice formulation, we briefly recall the definition of the gluon field in continuum Yang-Mills theory. For simplicity, we will consider the case of SU(2) Yang-Mills theory.

Under a gauge transformation of the fundamental matter field, i.e.

$$q(x) \rightarrow q^0(x) = U(x) q(x); \quad U(x) \in SU(2); \quad (1)$$

the gluon fields transform as

$$A^{a0}(x) = O^{ab}(x) A^b(x) + \frac{1}{2} \epsilon^{aef} O^{ec}(x) \theta O^{fc}; \quad (2)$$

$$O^{ab}(x) := 2 \text{trf}(x) t^{a-y}(x) t^b g; \quad O^{ab}(x) \in SO(3); \quad (3)$$

Let us stress that the gluon fields transform according to the adjoint representation while the matter fields are defined in the fundamental representation.

Let us compare these definitions of fields with the ones in LGT. In LGT, a discretization of space-time with a lattice spacing a is instrumental. The 'actors' of the theory are SU(2) matrices $U(x)$ which are associated with the links of the lattice. These link variables transform under gauge transformations as

$$U^0(x) = U(x) U^y(x+a) \quad U(x) \in SU(2); \quad (4)$$

For comparison with the ab initio continuum formulation, we also introduce the adjoint links

$$\mathcal{G}^{ab}(x) := 2 \text{trf} U(x) t^a U^y(x) t^b g; \quad (5)$$

$$\mathcal{G}^0(x) := O(x) \mathcal{G}(x) O^T(x+a); \quad O(x) \in SO(3); \quad (6)$$

where $O(x)$ was defined in (3).

In order to define the gluonic fields from lattice configurations, we exploit the behavior of the (continuum) gluon fields under gauge transformations (see (2)), and identify the lattice gluon fields $A^a(x)$ as algebra valued fields of the adjoint representation, i.e.

$$\mathcal{G}^{\text{adj}}(x) = : \exp \left[i g \sum_a A^a(x) t^a \right] ; \quad t^a_{bc} = -if^abc ; \quad (7)$$

where the total anti-symmetric tensor f^{abc} is the generator of the SU(2) group in the adjoint representation, and where a denotes the lattice spacing.

For later use, it is convenient to have an explicit formula for the (lattice) gluon fields $A^a(x)$ defined by (7) in terms of the SU(2) link variables $U(x)$. Usually, these links are given in terms of four {vectors of unit length

$$U(x) = u^0(x) + i \mathbf{u}(x) \cdot \boldsymbol{\tau} ; \quad [u^0(x)]^2 + [\mathbf{u}(x)]^2 = 1 ; \quad (8)$$

where τ^b are the Pauli matrices. Inserting this representation for $U(x)$ into (5) and using that $\mathbf{u}(x) = O(a)$, one finds

$$A^b(x) a + O(a^2) = 2 u^0(x) u^b(x) ; \text{ without summation over } b ; \quad (9)$$

Let us emphasize that this gauge field $A^b(x)$ has been defined by the adjoint link (7). The main difference to the former definition [23] of the gluon field is that the derivation of (9) does not assume that $u^0(x)$ is close to the unit element, i.e. $u^0(x) = 1 + O(a)$, but employs the somewhat weaker assumption that $u^0(x)$ must approach a center element in the continuum limit, i.e. $(u^0)^2(x) = 1 + O(a^2)$.

Finally, we illustrate the definition (9). Let us assume that we have exploited the gauge degrees of freedom (see (4)) to bring the SU(2) link elements $U(x)$ as close as possible to the unit matrix (which corresponds to the Landau gauge; see next subsection)

$$(x) : \sum_{f \in \text{lg}} \text{tr} U^0(x) \rightarrow \text{max} ; \quad (10)$$

In this gauge, we decompose the link variables by

$$U^0(x) = Z(x) \exp \left[i A^b(x) t^b \right] ; \quad (11)$$

where $A^b(x)$ is implicitly defined by (7) and $Z(x) = 1 / \sqrt{2 \text{tr} U^0(x)}$. Indeed, the lattice gluon fields (9) do not change when $U(x) \rightarrow (1)U(x)$. Hence, the fields $A^b(x)$ live in the SO(3) coset space. We here propose to

disentangle the information carried by the center and coset parts of the link variables by studying the $Z(x)$ and $A^b(x)$ correlation functions independently. We stress, however, that in Landau gauge (10) the role of the $Z(x)$ is de-emphasized ($Z(x) \neq 1$). For this reason, we do not expect a vastly different gluon propagator when the more standard definitions of the lattice gluon fields in terms of the fundamental links $U(x)$ are used [24, 23].

2.2 Gauge fixing

In the ab initio continuum formulated Yang-Mills theory, a frequently used gauge (in particular in connection with the Dyson-Schwinger approach) is the Landau gauge

$$\partial_\mu A^{0a}(x) = 0; \quad (12)$$

which is implemented by means of the Faddeev-Popov method, thereby relying on the assumption that the Faddeev-Popov determinant represents the "volume" of the gauge orbit specified by its representative $A^{0a}(x)$. This method is correct if the gauge condition picks a unique solution (x) of (12) for a given field $A^a(x)$. Unfortunately, the Landau gauge condition generically admits several solutions depending on the "background field" $A^b(x)$ (Gribov ambiguity). Further restrictions on the space of possible solutions (x) are required [25]. It was argued in [18] that the Faddeev-Popov method is not always justified if Gribov ambiguities are present.

Let us contrast the continuum gauge fixing with its lattice analog. In a first step, link configurations $U(x)$ are generated by means of the gauge invariant action without any bias to a gauge condition. In a second step, the gauged ensemble is obtained by adjusting the gauge matrices (x) (see (4)) until the gauged link ensemble satisfies the gauge condition. Obviously, this procedure correctly estimates the "volume" of the gauge orbit corresponding to the gauged configuration, and gauge invariant quantities which are calculated with the gauged configurations evidently coincide with the ones obtained from ungauged configurations.

However, this does not dispense us from dealing with the Gribov ambiguity. Let us illustrate this point: The naive Landau gauge condition for the lattice gluon field, i.e.

$$\partial_\mu A^{0b}(x) = 0 \quad (13)$$

is satisfied if we seek an extremum of the variational condition (10). If we restrict the variety of solutions (x) which extremize (10) to those solutions which maximize the functional (10), we confine ourselves to the case where

the Faddeev-Popov matrix is positive semi-definite. The corresponding fraction of the configuration space of gauge fields A^{ob} is said to lie within the first Gribov horizon. However, there is still a variety of possible gauge transformations (x) which all correspond to local maxima of the functional (10). A conceptual solution which resolves this residual Gribov ambiguity is to restrict the configuration space of gauge fields A^{ob} to the so-called fundamental modular region. In the lattice simulation, this amounts to picking the global maximum of the variational condition (10). In practice, finding the global maximum is a highly non-trivial task. A numerical algorithm which obtains the gauge transformation matrices (x) from the condition (10) might fail to locate the global maximum, and the numerical simulation might still sample a particular set of local maxima. Different algorithms might lead to different local maxima, and, hence, implement different gauges.

Here, we will study two extreme cases of gauge fixing: firstly, we will implement a gauge by means of an iteration over-relaxation algorithm which almost randomly averages over the local maxima of the variational condition (10) (IO gauge). The resulting gluon propagator will then be compared with the gluon propagator of a gauge where a simulated annealing algorithm searches for the global maximum (SA gauge). It will turn out that the gluon propagators of both gauges agree within statistical error bars. These observations indicate that the gluon propagator does not depend on the subset of configurations which we choose from the first Gribov domain.

2.3 Form factor calculations

The link configurations are generated using the Wilson action. We refrain from using a "perfect action" since we are interested in the gluon propagator in the full momentum range; simulations using perfect actions recover a good deal of continuum physics at finite values of the lattice spacing at the cost of a non-local action. For practical simulations, perfect actions are truncated which becomes an unjustified approximation at high energies where the full non-locality of the action must come into play.

In the present paper, most of the calculations were performed using a $16^3 \times 32$ lattice. The dependence of the lattice spacing on β (renormalization), i.e.

$$a^2(\beta) = 0.12 \exp\left(\frac{6.2}{11}(\beta - 2.3)\right); \quad \beta = (440 \text{ MeV})^2; \quad (14)$$

is appropriate for $\beta \in [2.1; 2.6]$ for the achieved numerical accuracy. Given (14), it is straightforward to calculate the extension of the lattice in one

direction, i.e. $L_x = N_x a$, where N_x is the number of lattice points in x -direction. In order to estimate the momentum range which is covered by the actual simulation, it is convenient to introduce the UV-cutoff by $\Lambda = \pi/a$. Table 1 provides L_t and Λ for $N_t = 32$.

Once gauge-fixed ensembles are obtained by implementing a variational gauge condition (see discussion of previous section), the gluon propagator is calculated using

$$D^{ab}(x, y) = \langle h A^a(x) A^b(y) \rangle_{MC}; \quad (15)$$

where $A^a(x)$ is defined in terms of the coset part of the link (see (9)). The Monte-Carlo average is taken over 200 properly thermalized gauge configurations. Of particular interest is the Fourier transform of this propagator which is defined by

$$D^{ab}(\hat{p}) = a^4 \sum_x D^{ab}(x) \exp(i\hat{p}x); \quad \hat{p}_k = \frac{2}{N_k a} n_k; \quad (16)$$

where n_k labels the Matsubara mode in k -direction and where N_k is the number of lattice points in this direction. It is also convenient to define the lattice momentum p by

$$p_k = \frac{2}{a} \sin \frac{\pi}{N_k} n_k; \quad (17)$$

which coincides with the Matsubara momentum \hat{p}_k in (16) in the limit $n_k \rightarrow N_k$. The definition (17) has the advantage that e.g. the free lattice propagator takes the familiar form $1 = p_k p_k$.

From perturbative Yang-Mills theory, one expects that the deviation of the full propagator from the free one is logarithmically small for large p^2 . In order to work out the non-trivial information of the Yang-Mills dynamics on the propagator, it is useful to introduce the gluon form factor $F(p^2)$ by

$$D(\hat{p}) = \frac{F(p^2)}{p^2}; \quad D(\hat{p}) = \sum_{a_i} D^{aa}(\hat{p}) \quad (18)$$

which measures the deviation of the full propagator from the free one. Since in Landau gauge the propagator is diagonal in color and transversal in Lorentz space, the form factor $F(p^2)$ contains the full information.

2.4 Numerical method

In principle, the gluonic form factor can be obtained by the Fourier transform of the measured quantity (15). Note, however, that the propagator (15)

Table 1: Simulation parameters

	2.1	2.2	2.3	2.4	2.5
L [fm]	8.6	6.6	5.0	3.8	2.9
[GeV]	2.3	3.0	4.0	5.2	6.8

is a rapidly decreasing function in coordinate space implying that the physical information at large distance $|x - y|$ is washed out by statistical noise and that, therefore, the information on the low momentum behavior is lost. To overcome this deficiency, it was proposed in [26] to directly address the propagator in momentum space, i.e.

$$D(\hat{p}) = \frac{1}{N_{\text{all}}} \sum_{a; x} A^a(x) \cos(\hat{p}x) + \frac{1}{N_{\text{all}}} \sum_{a; y} A^a(y) \sin(\hat{p}y) \quad (19)$$

where N_{all} is the number of lattice points. By the help of the translational invariance, i.e.

$$A^a(x) A^b(y) = f(x - y);$$

one indeed finds from (19) that

$$D(\hat{p}) = \frac{1}{N_{\text{all}}} \sum_{a; x} A^a(x) A^a(0) \cos(\hat{p}x) \quad (20)$$

Since the function $D(\hat{p})$ also contains the trivial factor $1 = p^2$, which is also present in a free theory, a further increase of the numerical accuracy is achieved by directly addressing the form factor $F(p^2)$. For these purposes, we mostly choose the momentum transfer to $\hat{p} = (0; 0; 0; \hat{p}_4)^T$ without any loss of generality and define

$${}_{\tau}A(x) := A(x + a e_4) - A(x); \quad (21)$$

where e_4 is the unit vector in time direction. A straightforward calculation yields

$$F(\hat{p}_4^2) = \frac{1}{N_{\text{all}}} \sum_{a; x} {}_{\tau}A^a(x) \cos(\hat{p}x) + \frac{1}{N_{\text{all}}} \sum_{a; y} {}_{\tau}A^a(y) \sin(\hat{p}y) \quad (22)$$

where p_4 is the lattice momentum (17) in time direction. By sake of the ${}_{\tau}$ operators in (22) the free part, i.e. $1 = p^2$, of the propagator $D(\hat{p})$ is precisely canceled, and we are left with the quantity of interest $F(p^2)$. It turns out that Monte-Carlo average (22) allows for a high precision measurement of the form factor.

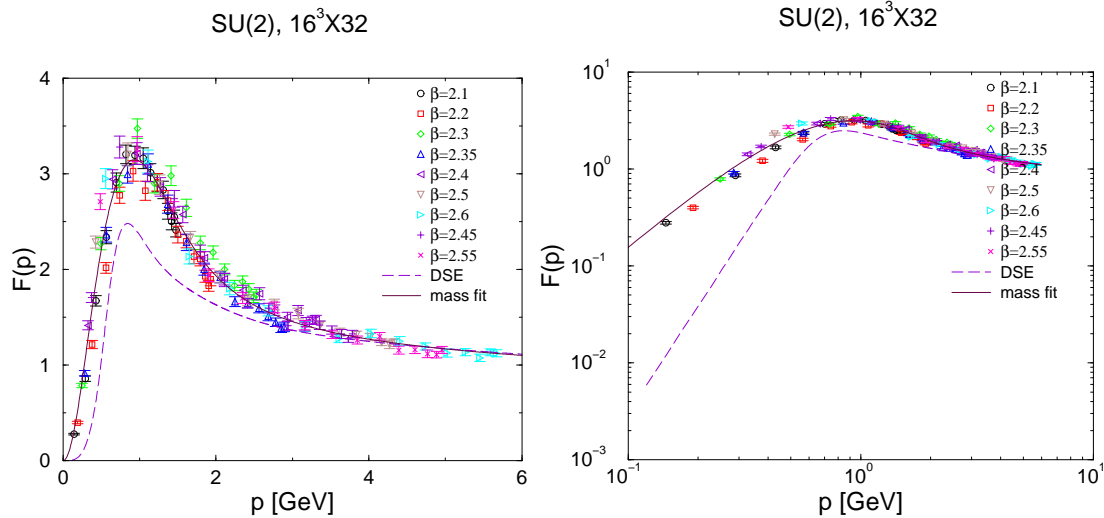


Figure 1: The gluonic form factor $F(p^2)$ as function of the momentum transfer (left panel: linear scale; right panel: log-log scale). Also shown is the solution of the set of DSEs proposed in [19] which have been solved for the case of SU(2) [27].

3 Numerical Results

3.1 Landau gauge

In this section, we will mainly use the iteration over-relaxation algorithm to implement the Landau gauge condition (10), and will refer to the corresponding gauge as IO-gauge. Later, we will also compare this gluonic form factor with one obtained in the SA-gauge where the gauge condition (10) is implemented by a simulated annealing algorithm.

In order to obtain the form factor $F(p^2)$ as function of the (lattice) momentum p (17), 200 properly thermalized configurations of a $16^3 \times 32$ lattice were used. Physical units for the momentum p (17) can be obtained by using (14). Calculations with different β -values correspond to simulations with a different UV-cutoff $\Lambda = \Lambda(\beta)$. In the first place, we obtain the unrenormalized form factor $F_B(p^2)$ as function of the momentum in physical units. The desired renormalized form factor $F_R(p^2)$ is obtained via multiplicative renormalization, i.e. $F_R(p^2) = Z_3^{-1} F_B(p^2)$. Thereby, the gluonic wave function renormalization $Z_3(\beta)$ is chosen to yield a finite (given) value for the renormalized form factor F_R at a fixed momentum transfer (renormalization point). In the following, we will suppress the subscripts of the

form factors, and $F(p^2)$ always refers to the renormalized form factor.

Figure 1 shows the result for the gluonic form factor in the IO-Landau gauge. Our reference scale is the string tension, which we set to $\sigma = (440 \text{ MeV})^2$ in order to assign physical units to momenta. The data for the renormalized form factor $F(p^2)$ which were obtained with different β -values nicely agree within numerical accuracy, thus signaling independence from the UV-cuto and the lattice volumes in the range shown in table 1.

At high momentum the lattice data are consistent with the behavior known from perturbation theory,

$$F(p^2) / \sigma = \log \frac{p^2}{\Lambda^2} \quad ; \quad p^2 \gg \Lambda^2 \quad (1 \text{ GeV})^2 : \quad (23)$$

Also shown in figure 1 is the coarse grained "mass t" (N, m_1, m_2, m_L, s fitted parameters; momentum p and all mass scales in units of 1 GeV)

$$F(p^2) = N \frac{p^2}{p^2 + m_1^2} \frac{1}{p^4 + m_2^4} + \frac{s}{[\log(m_L^2 + p^2)]^{13=22}} \quad (24)$$

which nicely reproduces the lattice data within the statistical error bars for

$$\begin{aligned} N &= 8.1133 ; & m_1 &= 0.64 \text{ GeV} ; & m_2 &= 1.31 \text{ GeV} ; \\ s &= 0.32 ; & m_L &= 1.23 \text{ GeV} ; \end{aligned} \quad (25)$$

Note that the multiplicative renormalization only affects the normalization N implying that the other fitting parameters are renormalization group invariant quantities.

Let us point out that an effective gluonic mass was introduced in [28] on phenomenological grounds. Gluonic masses were realized as electric and magnetic screening masses in the high temperature phase of $SU(2)$ YM-theory [29], and were also reported in the maximal Abelian gauge [30]. Note, however, that the description of the propagator in terms of two conjugate mass poles seems adequate for the Coulomb gauge [31].

3.2 Comparison with DSE solutions

Despite more than twenty years of successful hadron phenomenology originating from the quark [16, 17] and gluon [32, 33, 34] DSE, respectively, the coupled set of continuum DSEs for the renormalized gluon and ghost propagators has only recently been addressed in [19] and subsequently in [20, 21, 22].

In ref. [19], it was firstly pointed out that, at least for a specific truncation scheme, the gluon and ghost form factors satisfy scaling laws in the infra-red momentum range, in particular

$$F(p^2) \sim p^{-2} ; \quad p^2 \sim \Lambda_{\text{QCD}}^2 ; \quad (26)$$

Depending on the truncation of the tower of Dyson equations and on the angular approximation of the momentum loop integral, one finds $\beta = 0.92$ [19] or $\beta = 0.77$ [20] or $\beta = 1$ [21]. The lattice data are consistent with $\beta = 0.5$ corresponding to an infra-red screening by a gluonic mass (see figure 1 right panel). Interestingly, the prediction that the running coupling strength

$$g^2(p^2) = g^2(\mu^2) F(p^2) G^2(p^2) ; \quad G(p^2) : \text{Ghost form factor} \quad (27)$$

approaches a constant in the limit $p^2 \rightarrow 0$ is independent of the truncation and approximations used in [19, 20, 21, 35].

A feature of full Yang-Mills theory is multiplicative renormalizability (MR) which guarantees that the form factors $F(p^2)$ and $G(p^2)$ might be rescaled independently to satisfy the renormalization condition $F(\mu^2) = 1, G(\mu^2) = 1$ (renormalization point). Above, we have made use of this feature to obtain the renormalized form factor $F(p^2)$ from that lattice data for several values of β . It turned out that the truncations studied so far in [19, 20, 21] violate multiplicative renormalizability to a certain extent (see [20] and [22] for detailed discussions). Progress was made in [22] where a system of renormalized coupled gluon ghost DSEs were derived which manifestly reflect MR. Unfortunately, a self-consistent solution to this set of DSEs has not yet been obtained.

For a quantitative comparison of our lattice data with the SU(2) DSE solution, we refer to the truncation scheme of [19] which incorporates Taylor-Slavnov identities to some extent. In this approach, the running coupling at the renormalization point serves as an input to assign physical units to the momenta. Assuming an approximate MR, the solution for $F(p^2)$ is then rescaled to satisfy $F(\mu^2) = 1$. The final result is compared with the form factor obtained by our lattice calculations.

The DSE approach requires a knowledge of the scale Λ_{QCD} which is (to one loop accuracy) defined by (see e.g. [36])

$$F(p^2) = F(\mu^2) \frac{\ln \mu^2 = \frac{2}{\Lambda_{\text{QCD}}^2}}{\ln p^2 = \frac{2}{\Lambda_{\text{QCD}}^2}} ; \quad (28)$$

which holds for $p^2 \ll \Lambda_{\text{QCD}}^2$. Defining

$$F(p^2) = \frac{dF(p^2)}{dp^2} \Big|_{p^2=\Lambda^2} \quad (29)$$

and using (28), a straightforward calculation gives

$$\Lambda_{\text{QCD}}^2 = \Lambda^2 \exp \frac{13}{22} : \quad (30)$$

For the parameter set (25) which fits the lattice gluonic form factor with the string tension $\sigma = (440 \text{ MeV})^2$ as reference scale, Λ can be estimated from the t function (24). The renormalization point, $\Lambda = 6 \text{ GeV}$, was chosen to be part of the asymptotic momentum regime where both non-perturbative methods, i.e. LGT and the DSE approach, reproduce the known perturbative behavior. We finally obtain $\Lambda_{\text{QCD}} = 889 \text{ MeV}$, which is of the same order of magnitude than its SU(3) analog when the SU(3) gauge theory is equipped with the same string tension. At the renormalization point $\Lambda = 6 \text{ GeV}$, the running coupling constant for the SU(2) gauge theory is obtained by

$$g(\Lambda = 6 \text{ GeV}) = \frac{4}{22-3 \ln(\Lambda^2 = \Lambda_{\text{QCD}}^2)} = 0.449 \quad (31)$$

Using (31) as input, the solution of the DSEs with the truncations of [19] was solved [27] for the case of the SU(2) gauge group¹ which yields the DSE result shown in figure 1. We find a qualitative agreement of the DSE solution with our lattice result. Given the varieties of exponents (26) depending on the truncations of the DSEs, we do not expect a detailed agreement of the form factor close to zero momentum. We point out that the peak of the form factor at the intermediate momentum range is also observed in the DSE approach, although there are quantitative deviations concerning its steepness.

3.3 Gluon propagator and confinement

In the so-called maximum center gauges [8], the role of the coset part of the links referred to as "gluons" for the infra-red physics is de-emphasized, and center vortices appear as physical degrees of freedom in the continuum limit [9]. In this gauge these vortices act as the confiners of the theory:

¹ We thank C. Fischer for communicating his DSE solution for the SU(2) case prior to publication.

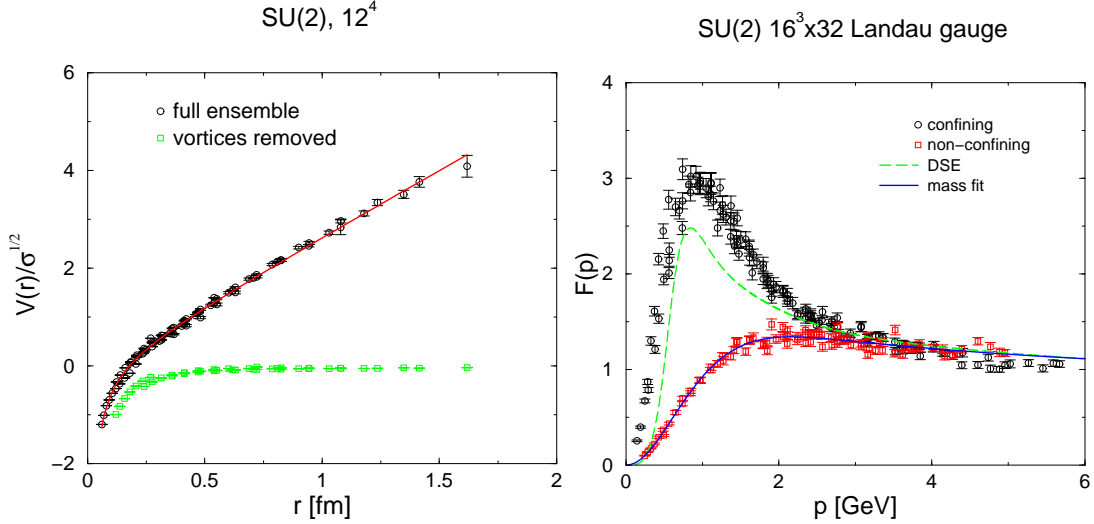


Figure 2: The static quark anti-quark potential (left panel) and the corresponding gluonic form factors (right panel); DSE solution from [27].

reducing the full Yang-Mills configurations to their vortex content still yields the full string tension [8], and, vice versa, removing these vortices from the Yang-Mills ensemble results in a theory with a vanishing string tension [8, 11].

In order to get a handle on the information of quark confinement encoded in the gluon propagator in Landau gauge, we firstly modify the SU(2) Yang-Mills theory to a theory which does not confine quarks, and, secondly, we compare the form factor of the gluon propagator of the modified theory with the full SU(2) result (see figure 1).

Let us briefly outline the numerical procedure for removing the confining center vortices from the Yang-Mills ensemble: firstly, we implement the maximal center gauge (MCG) condition (see (32) below) by an iteration over-relaxation algorithm [8], and obtain the Z(2) vortex links by center projection

$$U(\mathbf{x}) \stackrel{\text{MCG}}{\rightarrow} U^{\text{MCG}}(\mathbf{x}) \stackrel{\text{Proj}}{\rightarrow} Z(\mathbf{x}) = \text{sign} U^{\text{MCG}}(\mathbf{x}) :$$

The elements $Z(\mathbf{x})$ span an Z(2) gauge theory which contains the confining vortices as physical degrees of freedom. In order to remove the vortices from the full ensemble, we define configurations

$$U^{\text{mod}}(\mathbf{x}) := Z(\mathbf{x}) U(\mathbf{x}) :$$

The configurations $U^{\text{mod}}(\mathbf{x})$ do not yield quark confinement any more: the static quark anti-quark potential calculated from ensembles $U^{\text{mod}}(\mathbf{x})$ (see

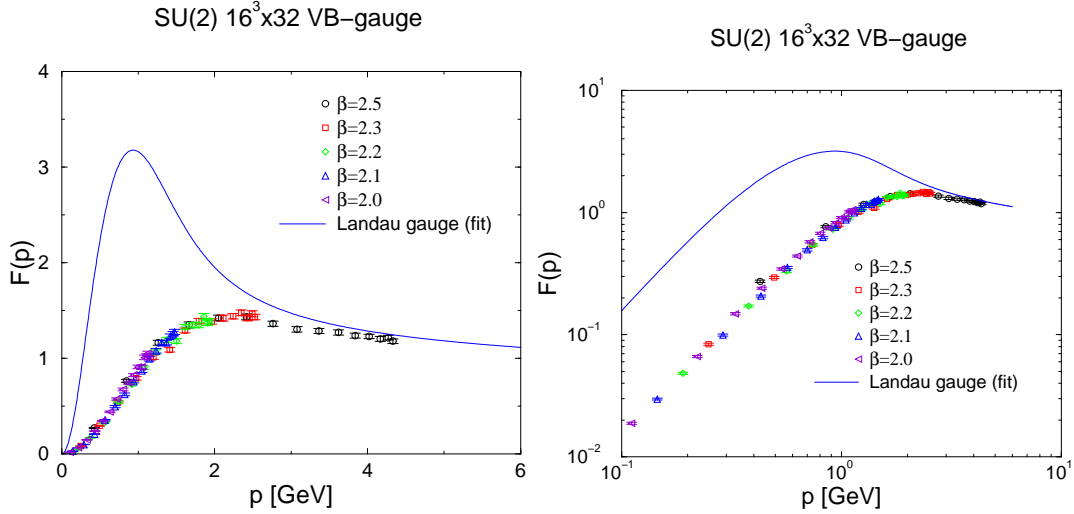


Figure 3: The gluonic form factor $F(p^2)$ in MCG as function of the momentum transfer (left panel: linear scale; right panel: log-log scale) for the case of IO-MCG.

Figure 2 left panel) illustrates that a removal of the center vortices produces a non-confining theory.

Finally, we implement the IO-Landau gauge condition on the configurations $U^{\text{mod}}(\mathbf{x})$ and calculate the corresponding renormalized form factor by the procedure outlined in the previous section. Figure 2 right panel shows this gluonic form factor obtained from the modified ensemble. The striking feature is that the strength of the form factor in the intermediate momentum range is drastically reduced.

3.4 Maximal center gauge

In the maximal center gauge [8]–[11], important parts of the infra-red physics is shifted to the vortex degrees of freedom. It is therefore instructive to investigate the residual information carried by the gluonic form factor in this gauge. The gauge transformations $\Omega(\mathbf{x})$ corresponding to MCG are obtained from the gauge condition

$$\Omega(\mathbf{x}) : \quad \text{tr} U^0(\mathbf{x}) = \max_{\Omega} \left| \int_{\text{fxg}} \text{tr} U^0(\mathbf{x}) \right| \quad (32)$$

We used an standard iteration over-relaxation algorithm [8] to calculate the matrices $\Omega(\mathbf{x})$ for a given "background" configuration $U(\mathbf{x})$.

A thorough study of the MCG in the continuum limit was performed in [37]. One finds that in the continuum limit the gauge condition (32) corresponds to a background gauge

$$[\partial + iA^B(x); A(x)] = 0; \quad (33)$$

where the background gauge field $A^B(x)$ is an optimally chosen center vortex field (see [37] for details). In the absence of center vortices in the considered gauge field $A(x)$, the gauge (33) coincides with the Landau gauge.

Once the gauge condition (32) is implemented, we used the gluon field definition (9) and eq.(22) to calculate the form factor. The result is shown in figure 3. We point out that the gauge condition (33) does not imply that the gluon propagator $D^{ab}(p)$ is transversal. Hence, the form factor (18) only provides parts of the information contained in the MCG gluon propagator. Here, we present the result for the form factor in MCG only for the purpose of comparison with the Landau gauge result.

By comparing figures 1 and 3 we observe that the form factors in Landau gauge and MCG drastically differ in the intermediate region. This is because in Landau gauge most of the information is accumulated in the adjoint (coset) part of the links while in the MCG the part of the non-perturbative content is shifted to its center part. Furthermore, comparing figures 2 and 3 we find that the gluon propagator in MCG basically agrees with the one where the center vortices are removed and the Landau gauge is subsequently implemented. This underlines the observation that in MCG confinement physics is relegated to center vortices.

3.5 The Gribov noise

Finally, let us check how strongly the gluonic form factor $F(p^2)$ depends on the choice of gauge, i.e. on the sample of minima of the variational condition (10) selected by the algorithm. For this purpose, we adopt an extreme point of view by comparing the gauge implemented by the iteration over-relaxation (IO) algorithm with the gauge obtained by simulated annealing (SA). The results obtained for the form factor in both cases are shown in figure 4. We find, in agreement with [24], that, in the case of the gluonic form factor, the Gribov noise is comparable with the statistical noise for data generated with $2 \times [2:1; 2:5]$ (scaling window).

4 Gluonic spectral functions

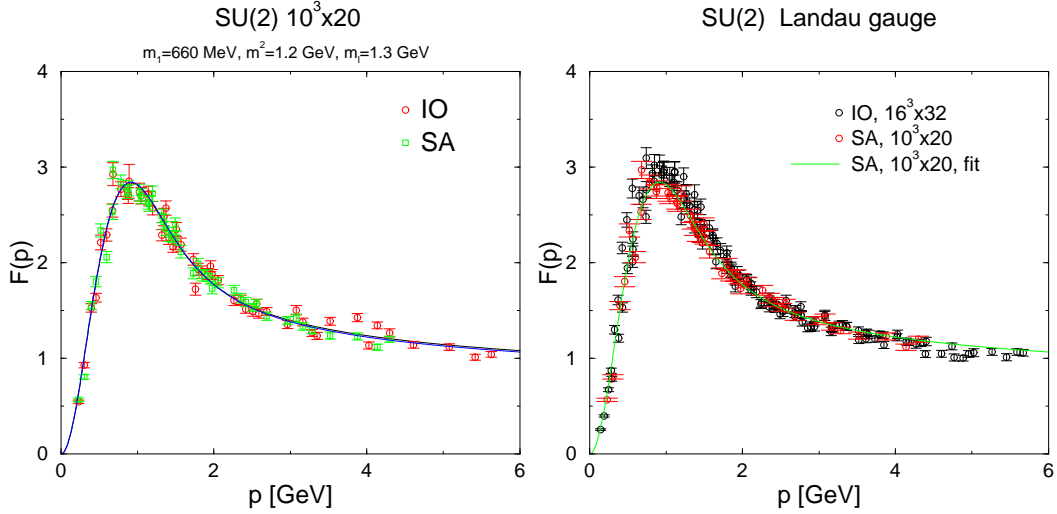


Figure 4: The gluonic form factor $F(p^2)$ for a $10^3 \times 20$ lattice in the gauge IO and SA, respectively (left panel) and compared with previous results (IO, $16^3 \times 32$) (right panel).

4.1 The spectral density

Let us consider the following spectral representation of the trace of the Euclidean propagator $D(p^2)$

$$D(p^2) = \int_0^{\infty} dm \frac{\rho(m)}{p^2 + m^2}; \quad (34)$$

where $\rho(m)$ is the spectral density. For example, the propagator of free particle with mass m_p is represented by a spectral density $\rho(m) = \delta(m - m_p)$. In general, the spectral density carries information on the strength with which single particle states contribute to the correlation function of interest. Hence, the spectral density must be positive if the space of physical particles is considered. Note, however, that this constraint must be abandoned if un-physical (while gauge dependent) correlation functions, e.g. the gluon propagator, is investigated. Moreover, the so-called negative norm states play an important role in Yang-Mills theory to circumvent the cluster decomposition theorem, what is inevitable to accomplish confinement of the theory. For a more detailed discussion of these issues see [17].

In order to study the contribution of hypothetical negative norm states to the gluon propagator, we will calculate the spectral density from the gluonic form factor

$$F(p^2) = \int_0^{\infty} dm \rho(m) \frac{p^2}{p^2 + m^2}; \quad (35)$$

Taking the derivative of $F(p^2)$ (15) with respect to p , one finds

$$F'(p^2) = 2p \int_0^Z dm^2 \rho(m^2) \frac{m^2}{(p^2 + m^2)^2} : \quad (36)$$

Hence, one immediately concludes that the form factor would be a monotonic function of the momentum if only positive norm states contribute, i.e. if $\rho(m^2) \geq 0$. An inspection of the results of the previous section shows that this is not the case for the gluon propagator.

Further insights are provided by the sum rules which are obtained from a large momentum expansion of the form factor (35), i.e.

$$F(p^2) = \sum_{n=0}^{\infty} c_n \frac{1}{p^{2n}} ; \quad c_n = (-1)^n \int_0^Z dm^2 \rho(m^2) m^{2n} : \quad (37)$$

where $n < n_c$ is restricted from above in order to guarantee the existence of the momentum integrals. In particular, we observe that

$$\lim_{p^2 \rightarrow \infty} F(p^2) = \int_0^Z dm^2 \rho(m^2) : \quad (38)$$

There is a substantial difference between the spectral function of a free massive particle and the one of Yang-Mills theory: while in the free particle case the form factor approaches unity at large momentum transfer, we know from perturbation theory that the Yang-Mills form factor vanishes at large momentum transfer. In view of (38), the crucial observation is that the free particle form factor $F(p^2 \rightarrow \infty) = 1$ is consistent with a positive definite spectral function, while the vanishing form factor $F(p^2 \rightarrow \infty) = 0$ in the Yang-Mills case implies that unless $\rho(m^2)$ vanishes identically it must change sign.

The remaining two subsections are devoted to numerically estimate the spectral function $\rho(m^2)$ from the form factor data in order to get insights into the qualitative behavior of the spectral function of a confining theory.

4.2 The generalized Maximum Entropy Method

In order to extract the spectral function $\rho(m^2)$ from our gluon propagator obtained in the lattice simulations we employ the Maximum Entropy Method (MEM). There is a wide span of applications for the MEM ranging from image modeling to solid state physics [38]. It was recently applied to reconstruct the spectral density of mesons from correlation functions obtained in lattice

calculations [39]. Since these applications use the positivity of the spectral density, a slight generalization of the MEM is necessary for our purposes.

Given the definition

$$f_{\text{MEM}}(p^2) := \int_0^{\infty} dm \, \rho(m) \frac{p^2}{p^2 + m^2}; \quad (39)$$

we define the MEM potential functional by

$$V[\rho] = \int dp \frac{1}{\rho(p)} \left(F(p^2) - f_{\text{MEM}}(p^2) \right)^2; \quad (40)$$

where $\rho(p)$ denotes the standard deviations of the measured values $F(p^2)$. For given $F(p^2)$, minimization of the functional $V[\rho]$ with respect to the spectral function $\rho(m)$ defined by (39) corresponds to a least square fit and would result in the optimal choice for $\rho(m)$ representing the data. However, it appears that substantial changes of the function $\rho(m)$ produce minor changes of the function $f_{\text{MEM}}(p^2)$ (39) which are comparable in size with the error bars of the measured function $F(p^2)$. In practice, the numerical algorithm which tries to minimize the potential (40) is unstable.

For circumventing this problem, one defines a MEM action functional

$$S[\rho] = S_{\text{entropy}}[\rho] + V[\rho] \quad (41)$$

where the parameter β regulates the influence of the entropy function $S_{\text{entropy}}[\rho]$ (to be specified below) on the minimum of the functional $S[\rho]$. The action functional (41) is minimized instead of the potential (40). Thereby, the entropy factor $S_{\text{entropy}}[\rho]$ is a measure for the deviation of the spectral density $\rho(m)$ from a default density $\rho_{\text{def}}(m)$. Whenever the potential term (40) is not conclusive on the precise form of the spectral density due to the size of the error bars, the numerical algorithm minimizes the deviations of $\rho(m)$ from the default model specified by $\rho_{\text{def}}(m)$. The entropy factor $S_{\text{entropy}}[\rho]$ is also used to encode constraints on the function $\rho(m)$. For instance, if one would like to insist on the positivity of the spectral function, the generic choice is [38]

$$S_{\text{entropy}}[\rho] = \int dm \, \rho(m) \log \frac{\rho(m)}{\rho_{\text{def}}(m)}; \quad (42)$$

since the functional (42) has a unique minimum for $\rho(m) = \rho_{\text{def}}(m)$.

For each value β a minimum of the action (41) exists for properly chosen entropy functionals. Let $\rho_{\beta}(m)$ denote the function which minimizes (41), and

let $s(\cdot)$ be the corresponding minimum value. The most probable spectral function is then defined by

$$\rho_{\text{av}}(m) = \frac{1}{N} \int d^n \phi \rho(m) \exp(-s(\cdot)); \quad N := \int d^n \phi \exp(-s(\cdot)); \quad (43)$$

Of course, it is mandatory to check that $f_{\text{MEM}}(p^2)$ (39) which is calculated with $\rho_{\text{av}}(m)$ does indeed represent the data $F(p^2)$ within statistical error bars.

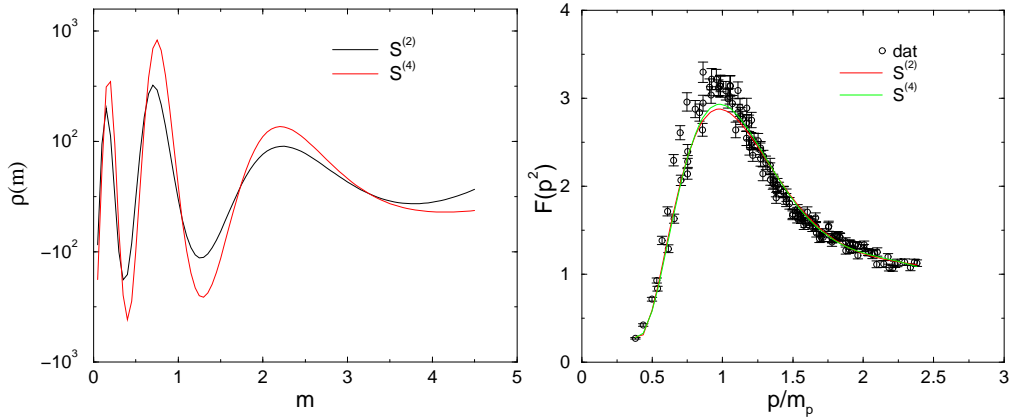


Figure 5: The spectral functions obtained with the entropy functionals $S^{(2)}$ and $S^{(4)}$, respectively, (left panel) and the corresponding form factors (right panel).

Since we must abandon the positivity constraint, we cannot use the standard entropy functional (42). We will here explore the two functionals

$$S_{\text{entropy}}^{(2)}[\rho] = \int dm \frac{h_d(m) i_2}{dm}; \quad (44)$$

$$S_{\text{entropy}}^{(4)}[\rho] = \int dm \frac{h(m) i_2}{\text{def}(m)}; \quad (45)$$

where we use a "default model" which suppresses the density $\rho(m)$ at small and at high values of m , e.g.

$$\text{def}(m) = \frac{m^2}{m^4 + (2m_p)^4}; \quad (46)$$

where the mass scale is chosen to be $m_p = 1 \text{ GeV}$. The first functional suppresses large gradients and, hence, ensures that the spectral function is

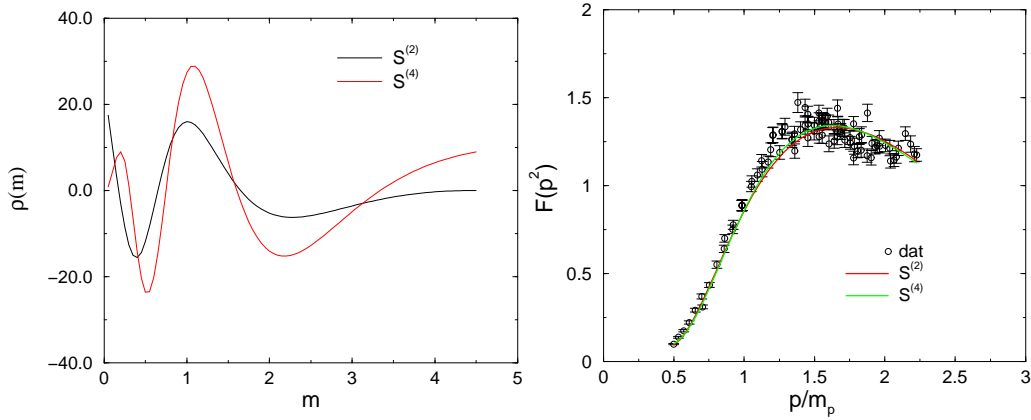


Figure 6: Same as figure 5 for the case of the non-confining Yang-Mills ensemble.

smooth. The second functional allows for large gradients, but minimizes the deviation of the spectral function from that of a "default model". The two functionals have been tested for the case of the form factor of a free particle (see appendix). The spectral function of the cases (45) and (46), respectively, have been compared with the result produced with the standard entropy functional (42). Since less information is supplied for the choices (45, 46), the exact infinite volume density is reproduced to less accuracy than in the case using the standard entropy functional (42). These results stress the importance of the physical constraints on the spectral function. We point out that, unless additional information on the spectral function of the gluon form factor is obtained and is used to constrain the latter, one must accept the uncertainty which becomes visible if two different entropy functionals (such as (45) and (46) are used.

4.3 MEM fit of the lattice form factor

In a first step, we do not attempt to supplement additional physical information to the MEM approach, but produce a direct MEM fit of the form factor data by using the two completely different entropy functionals (44), (45) in order to get a clue about the residual freedom in the choice of the spectral function $\rho(m)$. Our findings for the spectral function corresponding to the form factor $F(q^2)$ of the gluon propagator in Landau gauge is summarized in figure 5. The MEM approaches which employ the entropy functionals (44), (45) produce qualitatively the same result for the spectral function: $\rho(m)$ is a rapidly oscillating function of m .

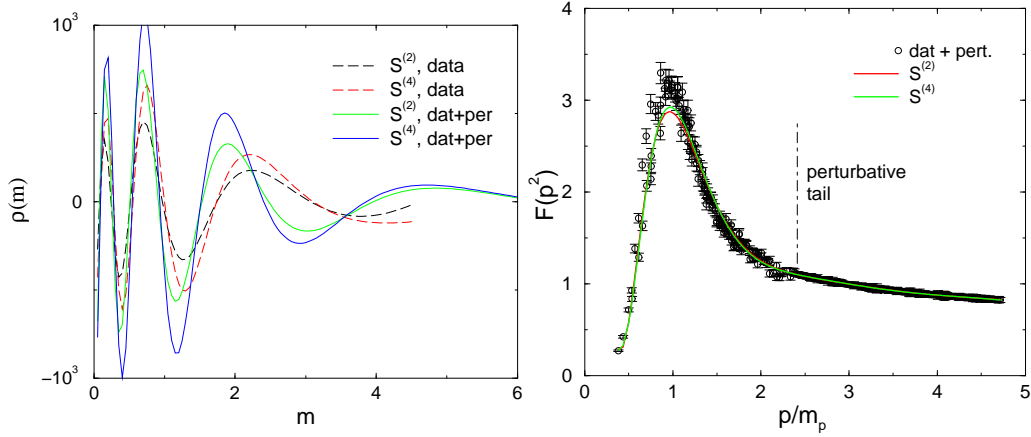


Figure 7: Same as figure 5 for the case that the perturbative tail has been added (full Yang-Mills ensemble).

We compare these findings with the ones obtained from the modified Yang-Mills ensemble from which the center vortices have been removed by the method described in the previous section. As shown there, the modified ensemble is non-confining. Since in this case, as in the case of the full ensemble, the form factor is non-monotonic due to the perturbative tail, negative norm states are inevitable. The MEM fit to the data indeed shows an oscillation of the spectral function $\rho(m)$ the amplitude of which is, however, orders of magnitude smaller than in the case of the full Yang-Mills theory (see figure 6).

Finally, we will assume that the perturbative regime is already approached at the upper limit of the momentum range which has been explored by the lattice calculation so far. Therefore, we will artificially extend the momentum range of the form factor by attaching the perturbative tail to the high momentum form factor obtained from the lattice data. In addition, we add a Gaussian noise to the perturbative tail. The noise is of the same order of magnitude as the statistical error bars, and specifies the degree of freedom which the MEM method might exploit to reproduce the form factor data.

Figure 7 shows the result for the spectral function for the case of the full Yang-Mills gluonic form factor. Most important is the observations that the oscillations are stable in the position. There is an enhancement of the amplitudes which is naturally expected if the momentum range of the data grows.

We also repeated the analysis of the spectral function for the case of the non-confining ensemble (see figure 8). Also in this case, we find that the

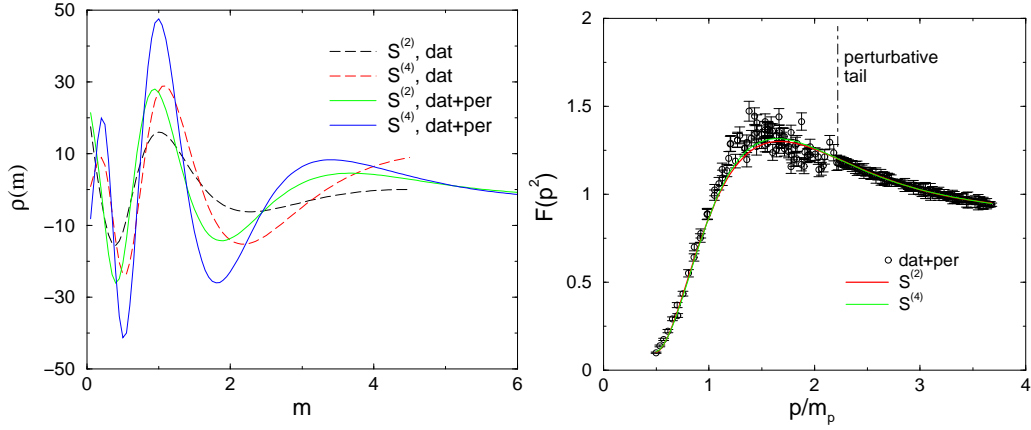


Figure 8: Same as Figure 5 for the case that the perturbative tail has been supplemented to the lattice data (modified non-conforming ensemble).

attachment of the known perturbative behavior at large momentum transfer does not qualitatively change the behavior of the spectral function (ρ), but results in an enhancement of the amplitude.

4.4 Infra-Red enhancement and negative norm states

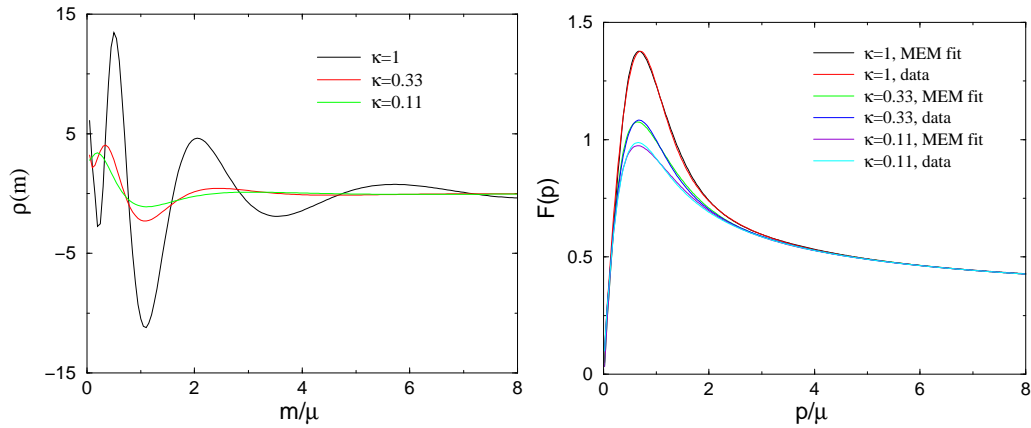


Figure 9: Spectral functions corresponding to the model form factors $F(p^2)$ (47) for several values of the infra-red strength.

In order to detect the origin of the rapid oscillations in the spectral density (ρ) for the case of the full gluonic form factor (see Figure 5), we are guided

by the mass t (24) of the lattice study and take the class of functions, i.e.

$$F(p^2) = \frac{p^2}{p^2 + m_1^2} \frac{h}{p^4 + m_2^4} + \frac{1}{\log \frac{m_2^2}{2} + \frac{p^2}{2}} \frac{i}{i_{13=22}} ; \quad (47)$$

where $m_1 = 0.64$, $m_2 = m_L =$ (varying), as a model for the gluonic form factor. Here, h controls the medium infra-red strength of the form factor. The MEM of the form factors which employ the entropy functionals $S^{(2)}$ are shown in figure 9 for $\beta = 1.033; 0.11$. These fits of the form factor fall on top of model functions $F(p^2)$ within plotting accuracy. The corresponding spectral functions are also shown in 9. One observes that amplitude of the oscillations of $\rho(m)$ increases if the infra-red strength, i.e. h , rises.

5 Conclusions

We have studied the gluonic form factor $F(p^2)$ in Landau gauge and maximal center gauge, respectively, by means of the continuum extrapolated SU(2) lattice gauge theory. The gauge field has been defined from the adjoint link variables. It is well known [25] that the Landau gauge condition (10) does not completely fix the gauge, but one must select a subset of configurations lying within the first Gribov horizon. We have studied two such possibilities: firstly, an iteration over-relaxation algorithm (IO gauge) which averages over the configurations within the first Gribov horizon, and, secondly, simulated annealing which selects the configuration belonging to the fundamental modular region (SA gauge). Within the statistical error bars, both methods have yielded the same gluonic form factor.

Close to zero momentum transfer, the gluonic form factor is mass dominated where the mass is $\approx 650 \pm 20$ MeV (we used $p_0^- = 440$ MeV as reference). The uncertainty is due to statistical errors as well as due to Gribov ambiguities, i.e. using IO and SA-gauge, respectively. Our numerical results are stable against a variation of the UV-cutoff (i.e. $\beta = a$) and the physical volume by roughly an order of magnitude (see table 1). The data points of the form factor in the far infra-red were obtained by using lattice sizes of $L = 9$ fm. This volume corresponds to a topological mass $2 = L = 140$ MeV which is much smaller than the dynamical gluon mass $m_1 = 650$ MeV. This explains the small finite size effects on the form factor observed by our numerical simulation.

In the medium momentum range we have found a rather pronounced peak while at high momenta our numerical data nicely reproduce the result from

perturbative Yang-Mills theory. Our numerical data are well fitted over the whole momentum range by the formula (24) which might be useful for further phenomenological oriented investigations.

A focal point of our studies is the information on quark confinement which might be encoded in the gluon propagator in Landau gauge. By removing the condensing vortices from the ensemble by hand, we are left with an ensemble which does not confine quarks (see figure 2 left panel). After the implementation of Landau gauge, we have seen that a good deal of strength is removed in the medium momentum range. We have therefore established a relation of the infra-red strength of the gluonic form factor in Landau gauge and quark confinement.

We have compared our result for the gluonic form factor with that obtained by solving a truncated set of Dyson-Schwinger equations (DSE) in continuum formulated Yang-Mills theory [27]. The DSE result is in qualitative agreement with our findings, but does not reproduce the data on a quantitative level (except in high momentum, perturbative regime): the power law behavior of the form factor in the vicinity of zero momentum is different, and the peak of the intermediate momentum range is less pronounced given that both approaches give same results in perturbative momentum regime.

Finally, we have studied the gluonic spectral functions which reproduce the numerical data for the gluon form factor. Using sum rule techniques, it becomes clear that the spectral function necessarily comprises negative parts. Using a generalized version of the Maximum Entropy Method (MEM), we have found that this is the case for the full form factor as well as for the form factor obtained for the non-condensing ensemble. At a quantitative level, the spectral function corresponding to the full form factor shows large amplitude fluctuations while the amplitude of the oscillations in the case of the spectral function obtained from the non-condensing ensemble are moderate.

Acknowledgments. Helpful discussions with R. Alkofer, J. C. R. Bloch, C. Fischer, L. v. Smekal and P. Watson are greatly acknowledged.

A Generalized MEM method (example)

We will briefly investigate several proposals for the MEM entropy functional $S_{\text{entropy}}[\rho]$ in (41) for the case of the form factor of a free particle of mass m_p where noise has been supplemented to the form factor by hand to simulate

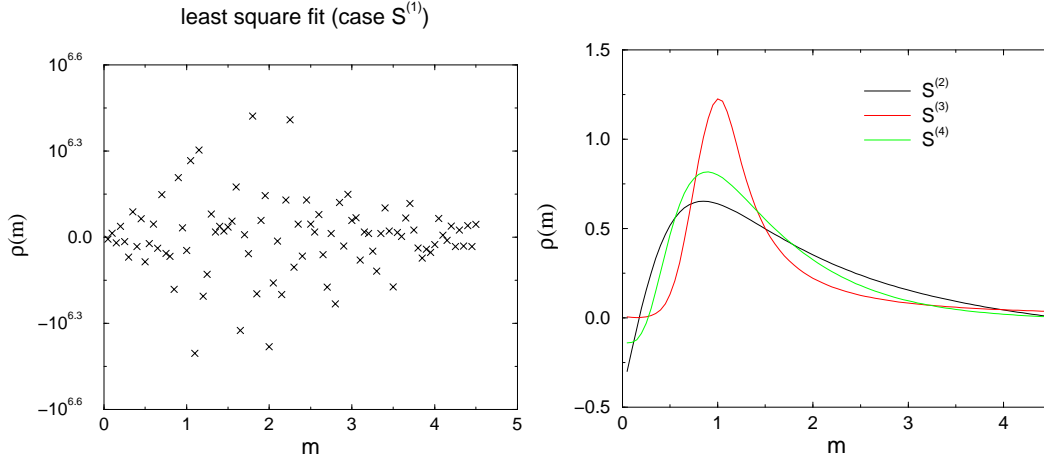


Figure 10: Possible spectral functions (differing by constraints) which fit the form factor of a free massive particle.

statistical uncertainties. The form factor is given by

$$F(p^2) = \frac{p^2}{p^2 + m_p^2} : \quad (48)$$

In order to illustrate the sensitivity of the spectral function $\rho(m)$ to the constraints, which are incorporated in $S_{\text{entropy}}[\rho]$, we will explore four different entropy functionals, i.e.

$$S_{\text{entropy}}^{(1)}[\rho] = \int_0^{\infty} \rho(m) dm ; \quad (49)$$

$$S_{\text{entropy}}^{(2)}[\rho] = \int_0^{\infty} \rho(m) \log \frac{\rho(m)}{\rho_{\text{def}}(m)} dm ; \quad (50)$$

$$S_{\text{entropy}}^{(3)}[\rho] = \int_0^{\infty} \rho(m) \log \frac{\rho(m)}{\rho_{\text{def}}(m)} dm ; \quad (51)$$

$$S_{\text{entropy}}^{(4)}[\rho] = \int_0^{\infty} \rho(m) \log \frac{\rho(m)}{\rho_{\text{def}}(m)} dm : \quad (52)$$

In order to perform the MEM program outlined in subsection 4.2, all integrals are converted Riemann sums. We used 135 data points representing $F(p^2)$ and N_m points to represent the spectral function $\rho(m)$.

The choice $S_{\text{entropy}}^{(1)}$ corresponds to a least square fit of the spectral sum $f_{\text{MEM}}(p^2)$ to the "measured" data. In this case, it turns out that the set of points $\rho(m)$ which represent the data set best is not a smooth function (see figure 10 for the case $m_p = 1$ and $N_m = 90$).

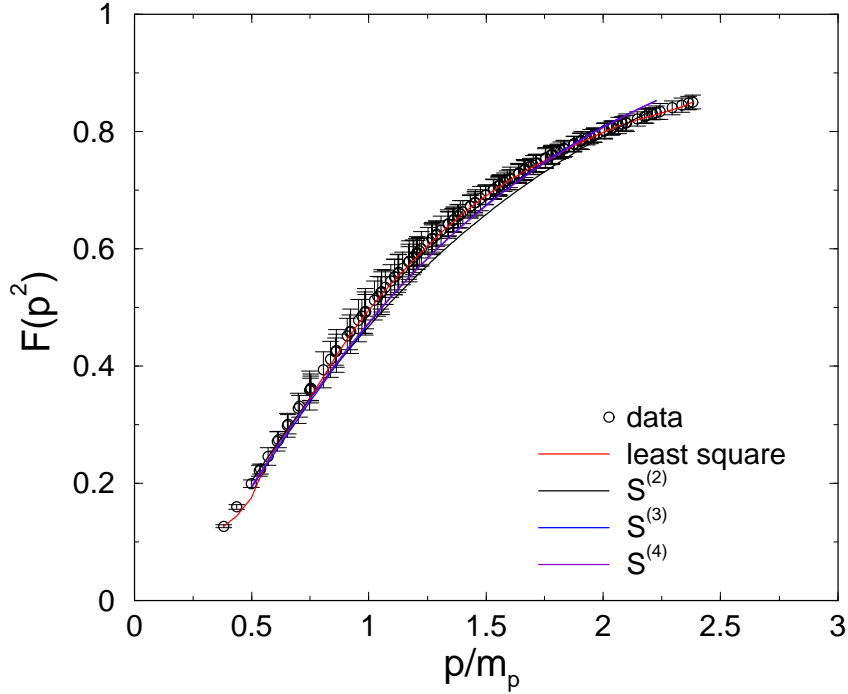


Figure 11: The form factor of a free massive particle fitted by several spectral functions.

The minimal requirement which we wish to incorporate in the spectral function $\rho(m)$ is that $\rho(m)$ is a smooth function of m . This is achieved by the entropy functional $S_{\text{entropy}}^{(1)}$ (50) which disfavors functions with large gradients. The spectral function is also shown in Figure 10 where we have chosen $N_m = 90$. One observes that a peak develops at $m = m_p$ approximating the exact infinite volume and zero noise spectral function $\rho_{\text{exact}} = \delta(m - m_p)$.

Let us compare, this result with the result of the standard approach demanding positivity. For this purpose, we use $S_{\text{entropy}}^{(3)}$ (51). This choice for the entropy functional does not constrain gradients. The smoothness of $\rho(m)$ is here incorporated by minimizing the difference to a smooth default density $\rho_{\text{def}}(m)$. Here, we used

$$\rho_{\text{def}}(m) = \frac{m^2}{m^4 + (2m_p)^4}; \quad (53)$$

which ensures that the spectral function vanishes for $m \rightarrow 0$ and $m \rightarrow 1$, respectively. This is the standard MEM approach to form factors with positive definite spectral functions.

Finally, we use an "Euclidean" norm to measure the difference of the spectral function with the default model (see $S_{\text{entropy}}^{(4)}$ [] (52)). Thus, the constraint to positivity is abandoned, and we, hence, expect that agreement of the MEM estimate of the spectral function with the exact result becomes worse. This is indeed observed (see figure 10).

We point out that all above MEM suggestions for the spectral function $\rho(m)$ fit the form factor $F(p^2)$ within the (artificial) statistical error bars. The best result for the spectral function is achieved with the entropy functional $S_{\text{entropy}}^{(3)}$ [] (51) which incorporates the most severe constraints, i.e. smoothness and positivity.

References

- [1] R. K. Ellis, W. J. Sterling, B. R. Webber, *QCD and Collider Physics*, Cambridge, 1996.
- [2] K. Langfeld, L. von Smekal and H. Reinhardt, *Phys. Lett. B* 362 (1995) 128.
- [3] G. S. Bali, V. Bomyakov, M. Müller-Preussker and K. Schilling, *Phys. Rev. D* 54 (1996) 2863.
- [4] G. 't Hooft, in *High Energy Physics* edited by A. Zichichi, (Bologna 1976);
G. 't Hooft, *Phys. Scripta* 25 (1982) 133;
S. Mandelstam, *Phys. Rept.* 23 (1976) 245.
- [5] P. Cea and L. Cosmai, *Nucl. Phys. Proc. Suppl.* 47 (1996) 318;
A. Di Giacomo, B. Lucini, L. Montesi and G. Pauti, *Phys. Rev. D* 61 (2000) 034504.
- [6] M. A. Lampert and B. Svetitsky, *Phys. Rev. D* 61 (2000) 034011.
- [7] K. Langfeld and A. Schafke, *Phys. Rev. D* 61 (2000) 114506.
- [8] L. Del Debbio, M. Faber, J. Greensite and S. Olejnik, *Phys. Rev. D* 55 (1997) 2298.
L. Del Debbio, M. Faber, J. Giedt, J. Greensite and S. Olejnik, *Phys. Rev. D* 58 (1998) 094501.
- [9] K. Langfeld, H. Reinhardt and O. Tennert, *Phys. Lett. B* 419 (1998) 317.

- [10] K. Langfeld, O. Tennert, M. Engelhardt and H. Reinhardt, Phys. Lett. B 452 (1999) 301.
M. Engelhardt, K. Langfeld, H. Reinhardt and O. Tennert, Phys. Rev. D 61 (2000) 054504.
- [11] P. de Forcrand and M. D'Elia, Phys. Rev. Lett. 82 (1999) 4582.
- [12] D. B. Kaplan, Phys. Lett. B 288 (1992) 342,
R. Narayanan and H. Neuberger, Phys. Lett. B 302 (1993) 62; Nucl. Phys. B 412 (1994) 574.
P. M. Vranas, Nucl. Phys. Proc. Suppl. 94 (2001) 177.
- [13] I. M. Barbour [UKQCD Collaboration], Nucl. Phys. A 642 (1998) 251.
- [14] J. Engels, O. Kaczmarek, F. Karsch and E. Laermann, Nucl. Phys. B 558 (1999) 307.
K. Langfeld and G. Shin, Nucl. Phys. B 572 (2000) 266.
- [15] C. D. Roberts and S. M. Schmidt, Prog. Part. Nucl. Phys. 45S1 (2000) 1.
- [16] C. D. Roberts and A. G. Williams, Prog. Part. Nucl. Phys. 33 (1994) 477.
- [17] R. Alkofer and L. von Smekal, in press by Phys. Rep., [hep-ph/0007355].
- [18] L. Baulieu and M. Schaden, Int. J. Mod. Phys. A 13 (1998) 985.
M. Schaden and A. Rozenberg, Phys. Rev. D 57 (1998) 3670.
- [19] L. von Smekal, R. Alkofer and A. Hauck, Phys. Rev. Lett. 79 (1997) 3591.
L. von Smekal, A. Hauck and R. Alkofer, Annals Phys. 267 (1998) 1.
- [20] D. Atkinson and J. C. R. Bloch, Phys. Rev. D 58 (1998) 094036.
- [21] D. Atkinson and J. C. R. Bloch, Mod. Phys. Lett. A 13 (1998) 1055.
- [22] J. C. R. Bloch, Multiplicative renormalizability of gluon and ghost propagators in QCD.

- [23] F. D. Bonnet, P. O. Bowman, D. B. Leinweber, A. G. Williams and J. M. Zanotti.
F. D. Bonnet, P. O. Bowman, D. B. Leinweber and A. G. Williams, *Phys. Rev D* 62 (2000) 051501.
- [24] A. Cucchieri, *Nucl Phys. B* 508 (1997) 353.
A. Cucchieri and T. Mendes, *Nucl Phys. Proc. Suppl.* 53 (1997) 811.
- [25] D. Zwanziger, *Nucl Phys. B* 412 (1994) 657.
- [26] D. Zwanziger, *Nucl Phys. B* 364 (1991) 127;
A. Cucchieri, *Phys. Rev. D* 60 (1999) 034508.
- [27] C. Fischer et al., in preparation.
- [28] M. Consoli and J. H. Field, *Phys. Rev. D* 49 (1994) 1293.
- [29] A. Cucchieri, F. Karsch and P. Petreczky, *Phys. Rev. D* 64 (2001) 036001;
Phys. Lett B 497 (2001) 80.
- [30] K. Amemiya and H. Suganuma, *Phys. Rev D* 60 (1999) 114509.
- [31] A. Cucchieri and D. Zwanziger, *Fit to gluon propagator and Gribov formula*, hep-lat/0012024.
- [32] S. Mandelstam, *Phys. Rev D* 20 (1979) 3223.
- [33] D. Atkinson, J. K. Drohm, P. W. Johnson and K. Stam, *J. Math. Phys.* 22 (1981) 2704; D. Atkinson, P. W. Johnson and K. Stam, *J. Math. Phys.* 23 (1982) 1917.
- [34] N. Brown and M. R. Pennington, *Phys. Rev. D* 39 (1989) 2723.
- [35] P. Watson and R. Alkofer, *Phys. Rev. Lett.* 86 (2001) 5239.
- [36] F. J. Yndurain, *Quantum Chromodynamics*, Springer-Verlag, 1983.
- [37] M. Engelhardt and H. Reinhardt, *Nucl Phys. B* 567 (2000) 249.
- [38] M. Jarrel, J. E. Gubernatis, *Phys. Repts.* 269 (1996) 133.
- [39] I. Wetzel and F. Karsch, hep-lat/0008008.